

1 **Wave structure and polarization electric field development in the bottom-side F**
2 **layer leading to post sunset equatorial spread-F**

3
4 Abdu¹, M. A., J. R. de Souza¹, E. A. Kherani¹, I. S. Batista¹, J. W MacDougall², J. H. A.
5 Sobral¹

6 ¹ Instituto Nacional de Pesquisas Espaciais, Sao Jose dos Campos, Brazil;

7 ² Department of Electrical Engineering, the University of Western Ontario, London,
8 Canada.

9
10 Abstract

11
12 In this paper we present the results of a study on the characteristics of large scale wave
13 structure in the equatorial ionospheric F region that serve as precursor to post sunset
14 development of the spread F/plasma bubble irregularities. The study is based on analysis
15 of Digisonde data from three equatorial sites in Brazil (Fortaleza, Sao Luis and
16 Cachimbo) for a period of about two months at a medium solar activity phase. Small
17 amplitude oscillations in the F layer heights, extracted at a number of plasma frequencies,
18 present characteristics as them being generated from upward propagating gravity waves.
19 They represent wave structures in polarization electric field having zonal scale of a few
20 hundred kilometers. Their amplitudes in the afternoon hours undergo amplification
21 towards evening, leading to post sunset development of ESF/plasma bubble irregularities,
22 on a statistical basis. On the days of their larger amplitudes they appear to occur in phase
23 coherence on all days, and correspondingly the evening prereversal vertical drift
24 velocities are larger than on days of the smaller amplitudes of the wave structure that
25 appear at random phase on the different days. The sustenance of these precursor waves
26 structures is supported by the relatively large ratio (approaching unity) of the F-region-to-
27 total field line integrated Pedersen conductivities as calculated using the SUPIM
28 simulation of the low latitude ionosphere. The significant amplification in the wave
29 structure towards sunset and the “phase coherent” nature of their occurrences on different
30 days, are explained tentatively on the basis of the spatial resonance mechanism.

32 1- Introduction

33 The plasma structuring of the nighttime equatorial F region, widely known as equatorial
34 spread F (ESF), is an important topic of investigation because of its impact on space
35 application systems as well as of the scientific challenge presented in explaining its
36 spatial structure and occurrence variability at different time scales, especially, at day-to-
37 day and short term scales. The instability leading to the plasma irregularity formation
38 develops typically through the Rayleigh-Taylor interchange mechanism, operating at the
39 steep bottom side gradient region of a rapidly rising post sunset F region. The enhanced
40 vertical drift of the layer (the post sunset rise) is due to the evening prereversal
41 enhancement in the zonal electric field (PRE), which therefore is a primary driver of the
42 ESF. Statistical as well as case studies have shown that the ESF occurrence depended on
43 the PRE vertical drift attaining a certain threshold value that varied with season and
44 longitude (Abdu, et al., 1983; Fejer et al., 1999; Kil et al., 2009; Carter et al., 2014).
45 Another requirement for the instability growth is the presence of a precursor seed
46 perturbation in the ambient electron density with associated polarization electric field.
47 The nature of the precursor seed perturbation is an important question especially in the
48 context of identifying the causes of the day-to-day variability widely observed in the ESF
49 occurrence. Wavelike patterns in the irregularity spatial structure, as observed by HF
50 radars, were attributed to upward propagating gravity waves originating from
51 tropospheric convective activity (Röttger, 1973). On a statistical basis the seasonal and
52 longitudinal patterns of the ESF occurrence have been attributed in part to gravity wave
53 generation sources associated to the ITCZ (Inter Tropical Convergence Zone) (McClure
54 et al., 1998; Tsunoda, 2010). Case studies have identified precursor signatures to
55 ESF/plasma bubbles development in the form of large scale wave structures (LSWS) in
56 the background electron density, as diagnosed from east-west scan incoherent scatter
57 radar measurements over Kwajelein (Tsunoda and White, 1981) or as additional F layer
58 traces (satellite traces) in ionograms, as observed by ionosondes (Lyon et al., 1961, Abdu
59 et al., 1981a, 2013; Tsunoda 2008; Li et al., 2012). A number of recent papers have
60 discussed the roles of the precursor conditions for the development of the ESF/plasma
61 bubble irregularities (see for example, Hysell et al., 2005; Abdu et al., 2009; Taori et al.,
62 2010; Li et al., 2012; Patra et al., 2013; Sridharan et al., 2014). Observations show also that

63 the verifiability of the role of a gravity wave precursor seed is subject to the dominance
64 of the other preexisting conditions. For example, Abdu et al (2009a) showed, based on
65 diagnostics by a Digisonde and a VHF radar, that the amplitude of the gravity wave
66 induced wavelike structures in the F layer heights during pre sunset hours that continued
67 their development into post sunset ESF growth, was dependent on the amplitude of the
68 PRE vertical drift. Such precursor wave structures are identifiable as the LSWS that have
69 also been observed in the form of longitudinal wave structure in ionospheric TEC as
70 observed from measurements on C/NOFS satellite passes discussed, for example, by
71 Thampi, et al., (2009), Tulasi Ram et al., (2012, 2013) and Tsunoda et al., (2011). In the
72 study by Abdu et al (2009a) the amplitude of the precursor wave structure required for
73 the ESF growth, was found to be larger (smaller) when the PRE vertical drift was smaller
74 (larger). An evaluation of the importance of a precursor seed for ESF development in a
75 given situation is therefore dependent, obviously, on the prevailing vertical drift as well
76 as other background conditions. In any case an important question concerns the day time
77 sustainability near the dip equator of a gravity wave induced structure in polarization
78 electric field, with its corresponding wave structure in electron density, that may continue
79 in strength to evening hours and onto post sunset ESF instability growth. In this paper we
80 address this important question for the first time, discussing the nature of the precursor
81 wave structure, its production by gravity waves, its relationship to the PRE and the nature
82 of the background ionospheric conductivity distribution that contributes to its sustenance
83 into the post sunset hours, leading to ESF development.

84

85 2- Data Analysis

86 The study is based on Digisonde data from three equatorial sites in Brazil. The F layer
87 heights selected at specific plasma frequencies (from 5 MHz to 8 MHz) from
88 measurements made at 5 to 10 minutes cadence are used in the study. Height values were
89 band-pass filtered to extract their oscillation amplitudes, as wave structures, within a
90 period band from 0.5 to 1.5hrs. The heights were also used to calculate the vertical drift
91 velocity as dhF/dt whose enhancement at sunset, due to the PRE, is evaluated in relation
92 to the corresponding precursor wave structure characteristics.

93

94 3- Results

95

96 Fig. 1(a) shows the band-pass filtered height oscillations between midday (15 UT =12
97 ST) and midnight mass plotted for the entire month of October 2001 over Fortaleza (3.9°
98 S, 38.45° W, dip angle: -9°). Although results are available at 4 frequencies (5, 6, 7 and 8
99 MHz) only those of 5 MHz and 8 MHz are shown here. The vertical drifts calculated as
100 the mean of the drifts at the four frequencies are also mass plotted in the bottom panel.
101 We note the presence of oscillations of significant amplitude (DhF) in the fixed plasma
102 frequency heights (reaching up to ~ 20 km peak-to-peak) starting from near midday and
103 increasing in amplitude towards sunset, a feature clearly seen at both 5 MHz and 8 MHz,
104 but better defined at the latter frequency, which represent a higher height. The
105 oscillations appear to present a dominant period in the range of ~1 to 1.5 hours (than in
106 the neighboring period bands that were also tried). In most cases the oscillations
107 continuing to post sunset hours evolve into spread F development as indicated by the grey
108 segment of each DhF curve. Only on five nights (02, 03, 11, 21 and 22 October) there
109 was no spread F occurrence till midnight; these are highlighted as continuing color curves
110 (without the grey segment). The vertical drift shows (bottom panel) that the prereversal
111 enhancement in its values peaked near 21:15 UT (18:43 LT), the mean drift velocity at
112 this time being ~ 50 m/s. The statistical onset time of the ESF for this period (October
113 month) indicated by the grey segment of the DhF curves, is found to be around 21:45
114 UT/19:13 LT. This onset time is close to and at the descending phase of the PRE vertical
115 drift, in good agreement with previous results (see for example, Abdu et al., 2014). It may
116 be noted that in the case of the five non spread F nights the PRE vertical drifts were
117 significantly smaller than on the SF nights, except on 21 October when the PRE drift was
118 large but did not cause any ESF development due to an intense magnetic disturbance that
119 occurred during the hours of normal SF growth. So we will not include this night in our
120 discussion. To make the comparison easier, we present in Fig. 1b the wave oscillations
121 and the vertical drift only for the non SF cases. We may note, between Fig. 1(a) and (b)
122 that the non SF days have generally lower wave structure amplitudes suggesting that the
123 lower amplitude of the seed perturbation is a key factor in the non occurrence of the
124 instability. Additionally, we note that the PRE vertical drifts are also significantly smaller

125 on these days. Thus, we find that clearly, both of these precursor conditions control the
126 ESF instability growth. An evaluation of the relative importance of either of these
127 precursor factors should necessarily involve instability modeling, which is considered for
128 a future study.

129

130 The results obtained from similar analysis performed for Sao Luis (2.33° S, 44.2°W, dip
131 angle: -5°), located some 600 km westward of Fortaleza, are shown in Fig. 1(c). We
132 may note that the major features of the DhF oscillations over Sao Luis are similar to those
133 over Fortaleza, but the amplitudes appear to be a bit smaller with the exception of one
134 day. The vertical drift amplitudes are also similar at the two sites. Over Sao Luis there are
135 six non SF nights for which the relative amplitudes of the wave structure and the PRE
136 vertical drift are similar to that presented over Fortaleza. We point out here one specific
137 case of 03 October for which SF did occur at 23 UT (20 LT) which is a very delayed
138 occurrence. For this case also the wave structure amplitude (the yellow curve running on
139 top in the upper two panels of Fig. 1c) is smaller than on the days of SF, and so was the
140 PRE vertical drift (shown in blue curve in bottom panel of Fig. 1c). Thus, the results are
141 consistent between Fortaleza and Sao Luis, for the cases of spread F non occurrence for
142 entire night, as well as for the case of SF delayed occurrence as late as 23 UT/20 LT.

143

144 Additional characteristics of these oscillations are presented in Fig. 2(a), which shows the
145 oscillations at all the four frequencies plotted, for some specific days, and in a way to
146 reveal any vertical phase propagation in these oscillations. In the top panel (25 October
147 2001) we note that, before sunset hours (near 21UT), the oscillation phase propagates
148 downward, thereby confirming the upward propagating gravity wave nature of these
149 height oscillations. It is important to note that the downward phase propagation feature is
150 not present any more with the onset of post the sunset SF, indicated by the beginning of
151 the shaded area (at 21:50 UT/ 19:18 LT). This change occurred as a result of the
152 dominance of the polarization electric field associated with the ESF bubble development.
153 In other words, the downward phase propagation that is a characteristic of the GW
154 induced height oscillation in the neutral background will not be present in the plasma
155 density height when a dominant role in driving such oscillations is played by polarization

156 electric field, which in this case did develop with the growth of the plasma bubble
157 instability. In many cases, the polarization electric field appears to control the height
158 oscillations even before the SF onset as can be noted from the absence of any downward
159 phase propagation near sunset in the example of 29 October (in the lower panel). In fact
160 the polarization electric field appears to control the height oscillation during the entire
161 period before sunset as seen from the total absence of the downward phase propagation
162 characteristics in the examples of 17 and 06 Oct, presented in the lowest two panels.
163 Upon checking all the individual days of October 2001 we found that the downward
164 phase propagation feature was absent on most of the days (similar to the two days
165 illustrated here). The reason for this can be explained as follows. The polarization electric
166 field driving these oscillations is subject to being field line mapped to the plasma
167 frequency heights at all the four frequencies and further to the underlying E region as
168 illustrated in Fig. 2(b). The situation depicted here is for the case of a gravity wave that
169 propagate zonally with its wave front aligned in the magnetic north-south so that its
170 wavelength in that direction is long enough, compared to the magnetic field line
171 curvature to a degree that the iso density lines of the radio wave reflection heights can be
172 considered as approximate straight lines. The dashed lines drawn horizontal represent the
173 corresponding reflection levels at the four plasma frequencies. As a result of the field line
174 mapping connecting these levels with the underlying E region of significant Pedersen
175 conductivity (during daytime), the polarization electric field can maintain the same phase
176 in an extended height region of F region flux tubes, depending upon the vertical wave
177 length of the GW. This situation can cause the different, but close by, reflection heights at
178 the four plasma frequencies to oscillate in the same phase. In this way a downward phase
179 propagation that might be present in the GW oscillations of the neutral background will
180 not be present in the resulting plasma density oscillations, as observed here. The height
181 oscillations that are due to vertical plasma motion should be produced by a zonal
182 polarization electric field that is induced by vertical perturbation wind of the gravity
183 wave. Thus, these results clearly demonstrate the generation of zonal polarization
184 electric fields by the vertical perturbation winds of a GW propagating zonally. In a more
185 general case we may expect to observe also vertical polarization electric field if the GW
186 propagation is in zonal and also slant upward directions.

187

188 For a different propagation direction the gravity wave front projected in the magnetic
189 meridian may correspond to the iso density surfaces presenting significant curvature.
190 When that curvature is nearly comparable to that of the field lines the polarization electric
191 field mapping will not connect the different density surfaces at the different plasma
192 frequencies in the region of our observation. This situation can be accompanied with a
193 possibly significant presence of perturbation meridional wind (depending upon the
194 magnetic field inclination of the observing location). In this case a downward phase
195 propagation feature should be observed, as seen in some of our results of Fig. 2a.

196

197 In Fig 2(a) we further note that the amplitude of the oscillation increase from midday
198 towards sunset. A clear example of this feature is illustrated in Fig.2(c) for 19 October
199 2001. Besides the clear increase of the oscillation amplitude towards post sunset hours
200 we note also that in this case the amplitude is smaller at the higher frequency (8 MHz)
201 that corresponds to a higher height, as compared to the 5 MHz that corresponds to a
202 lower height. The height difference varied from ~ 100 km to 60 km during this period.
203 But the examples of Fig. 2(a) present an opposite tendency. The significance of these
204 features will be discussed later. It may be argued here that the photochemistry of the F
205 layer that includes the ionization production (during daytime) and recombination could
206 be thought to affect the oscillation amplitude. However, since the contribution of these
207 factors to the plasma frequency (iso-density) height, as measured by the Digisonde, varies
208 at a relatively slow rate, without involving any oscillatory component, they are unlikely
209 to modify the measured oscillation amplitude. For example, the degree of any possible
210 effect can be thought of as being dependent on the value of the recombination time at a
211 given height relative to that of the wave oscillation period at that height, keeping in mind
212 that the effect of recombination is to cause upward displacement of an iso-electron
213 density height. It may be noted that the F region recombination time varies by 1-3 hours
214 in the height region (around 300 km) where these height oscillations (with period range
215 of 1-1.5 hours) are measured. A smaller recombination time than the oscillation period
216 will have the effect to make the measured oscillation amplitude to be an under-estimation
217 of the real downward height displacement in the negative phase of the oscillation cycle,

218 while being an over-estimation of its upward displacement in the positive phase of the
219 cycle, thus tending for a cancellation of the net effect in a complete oscillation cycle as
220 measured by the Digisonde. Therefore, we consider it very unlikely that the oscillation
221 amplitude in this study has been affected in any significant way by the photo-chemistry
222 of the F layer.

223

224 Sixty six days of data over the equatorial site Cachimbo (9.47° S, 54.83°W; dip: - 4.25°)
225 during the COPEX campaign period (Oct-December 2002) (Abdu et al., 2009b) was
226 analyzed, by separating the data into two groups. Group 1 (G1) consisted of all the days
227 selected by verifying that the DhF oscillation presented nearly the same phase (phase
228 coherence) on all the days. This is plotted in the upper panel in Fig. 3. The remaining
229 days constituting the Group 2, (G2), are mass plotted in the middle panel, which
230 obviously shows random phases on the different days. The mean of the F layer vertical
231 drift for the two groups G1 and G2, are plotted as red and blue curves, respectively, in the
232 bottom panel. The vertical drift on the individual days of the two groups was calculated
233 as the average of the $d(hF)/dt$ values at all the four frequencies. We may point out here
234 that the vertical drift values as deduced from the hF variation during the day hours are not
235 sufficiently reliable because of the dominant role of the photo-chemistry at these hours,
236 but approaching the sunset enhancement in the height, when it exceeds 300 km, (due to
237 the PRE), the drift velocities are very reliable (Bittencourt and Abdu, 1981). The results
238 in Figure 3 appear to be very interesting but also somewhat intriguing. The “coherent”
239 height oscillations of the G1 days clearly shows a period of ~1-1.5 hours, with amplitude
240 increasing towards the sunset, which leads to post sunset SF development in most cases
241 (as was noted also in Fig 1). The G2 days also show similar periodicity, but the
242 oscillation amplitudes are smaller with generally lower rate of amplification towards
243 sunset, which also lead to SF development in most cases. We note that the average
244 vertical drift peak near 22:30 UT/18:50 LT is significantly higher (by ~20 m/s) on the G1
245 days than on the G2 days. We may further note that around the period of the PRE peak
246 the oscillation phase on the G1 days (in top Panel), showing descending DhF values in
247 most cases, suggests an average vertical drift that is negative, which would add more
248 significance to the larger PRE vertical drift values for this case.

249

250 4- Discussion

251

252 The wave structure, manifesting itself as the height oscillations of the bottom-side F layer
253 during daytime, becomes amplified towards post sunset hours leading to ESF
254 development. This result, reported here for the first time, represents a unique feature of
255 the evening equatorial ionosphere that can offer important insight to a better
256 understanding of the conditions governing the post sunset ESF development. Although
257 the GWs driving the height oscillations may have perturbation winds in any of the three
258 cardinal directions depending upon its propagation vector, a meridional component, if
259 present, will not produce any electric field under the low inclination magnetic field
260 configuration characterizing the present observations. It is the vertical and zonal winds
261 associated with a GW propagating zonally, and in slant upward direction, that can
262 produce the polarization electric fields. Particularly, a vertical perturbation wind (ΔU_Z)
263 can produce the zonal polarization electric field (E_Y), through the relationship $E_Y = -\Delta U_Z$
264 $\times B_\theta$, that is responsible for the observed height oscillations. B_θ is the magnetic field
265 intensity. The zonal scale sizes of the wave structures can be estimated from their period
266 range (which is ~1-1.5 hrs.) and the corresponding phase velocity, which is not available
267 for this measurement. If we use phase velocities in the range of 100- 300 m/s, based on
268 the measurement of the TID (Travelling Ionospheric Disturbance) velocity made in a
269 nearby equatorial region by MacDougall et al. (2011) for October 2010, the zonal scales
270 come out to be in the range of 400-1200 km. The study based on Digisonde observation
271 by Abdu et al. (2009a) yielded a zonal scale length of the order of 400 km. These values
272 are compatible with the ranges of zonal wavelengths of the “large scale wave structure –
273 LSWS” as reported by Tsunoda and White (1981) and as obtained from the TEC
274 longitudinal variations measured from C/NOFS passes, mentioned previously (Thampi et
275 al., 2009; Tsunoda, et al., 2011; Tulasi Ram et al., 2012). Thus the large-scale wave
276 structure, which we call here also as precursor wave structure, appears to be a constant
277 feature of the equatorial F region in these measurements. An important question here
278 concerns the sustenance of the polarization electric field generated by gravity waves in
279 the daytime F region that is field line mapped to an E region of large daytime

280 conductivity, and how that can grow in amplitude towards sunset to impact on the post
 281 sunset ESF development. The sustenance of a gravity wave wind induced polarization
 282 electric field (of zonal direction in this case) in the F region (E_Y) should depend upon the
 283 ratio of the field line integrated conductivities of the E and F regions as given by:

284

$$285 \quad E_Y = -\Delta U_Z \square B_0 [\sum_F / (\sum_F + \sum_E)] \quad (1)$$

286 Where \sum_F and \sum_E are the field line integrated Pedersen conductivities, respectively, of the
 287 E - and F region segments of a field line (see also, Abdu and Brum, 2009). We calculated
 288 the values of the field line integrated conductivity segments, \sum_F and \sum_E , using an ion
 289 density distribution in altitude versus latitude (the latitude extending from dip equator to
 290 $\pm 20^\circ$ magnetic latitude). Such ion density distribution as a function of local time (or UT)
 291 was calculated using the Sheffield University Plasmasphere-Ionosphere Model (SUPIM)
 292 simulation runs (Bailey et al., 1997). For this calculation we used a SUPIM version that
 293 was modified to extend the lower height limit of calculation from its original 120 km
 294 down to 90 km. The conductivity ratio, $\sum_F / (\sum_F + \sum_E)$ that resulted from this calculation is
 295 plotted in Figure 4 (top panel) as a function of magnetic field line apex height up to 800
 296 km over equator versus local time.

297

298 In the lower two panels are plotted the local time variations (LT= UT- 3hours) in the
 299 following parameters: N_{e8MHz} , the electron density at the plasma frequency of 8MHz
 300 (corresponding to the wave structure plotted in Fig. 3), the monthly mean values of its
 301 heights (hF_{8MHz}) and that of the E layer peak density (NmE) for October 2001 over
 302 Fortaleza as well as the ratio $N_{e8MHz} / (N_{e8MHz} + NmE)$ (in the bottom panel). This latter
 303 parameter can serve as a rough indicator of the LT variation in the integrated conductivity
 304 ratio. We may note here that the height of the 8MHz plasma frequency (hF_{8MHz}) increases
 305 steadily during the post noon hours till it reaches a peak at 550 km after sunset (21:40
 306 UT). During this period the decrease in NmE results in an increase in the ratio of
 307 $N_{e8MHz} / (N_{e8MHz} + NmE)$ (bottom panel). We notice a corresponding trend also in the
 308 model simulation results as explained below. The modeled values of the integrated
 309 conductivity ratio (upper panel) during the post noon hours is generally quite significant
 310 being around 0.8 for the height region of our interest, around 280 km as judged from the

311 hF_{8MHz} values, thereby guaranteeing the sustenance of a major proportion (80%) of the
312 zonal polarization electric field produced by the perturbation wind as per Eq.1. If we
313 follow the conductivity ratio in the upper panel along a height variation similar to that of
314 the observed hF_{8MHz} variation, we notice that the ratio clearly increases towards sunset.
315 This feature appears to contribute to the sustenance of the polarization electric field, and
316 further, to some extent, to its amplification towards sunset such as that observed in Figs
317 1 and 3. It is not certain, however, if this factor (the conductivity ratio, that increase by a
318 factor of ~20%) alone could explain entirely the observed degree of amplification in the
319 wave structure amplitude that appears to be roughly close to a factor of two in Fig. 3.

320

321 There are two important, at the same time intriguing, aspects to the results in Fig. 3: (1)-
322 There appears to be a connection between the oscillations/wave structure amplitude and
323 the PRE vertical drift, a larger average evening vertical drift following a larger oscillation
324 amplitude; (2)- The oscillations of the G1 case are generally of larger amplitude, occur
325 coherently in phase on the different days, and have a larger rate of amplification towards
326 sunset. We do not have at this stage a definitive explanation for these rather intriguing
327 features, but a tentative/speculative one can be proposed as follows. The evening vertical
328 drift enhancement is known to arise from the sunset electrodynamic processes in which
329 the thermospheric zonal wind (directed eastward) and the local time/longitudinal gradient
330 (across the terminator) in the E layer conductivity play the major roles (Rishbeth, 1971;
331 Heelis et al., 1974, 2012; Farley et al., 1986; Batista et al., 1986, Eccles, 1998; Abdu and
332 Brum 2009; Richmond et al., 2015). While the longitudinal conductivity gradient at
333 sunset is dependent on the degree of alignment between the sunset terminator and the
334 magnetic meridian (Abdu et al., 1981b; Batista et al., 1986), it is also significantly
335 controlled by the E layer zonal winds arising from different upward propagating tidal
336 modes. Specifically, calculations of the E layer density variation at sunset under the
337 action of a tidal zonal wind have shown that the density longitudinal/local time gradient
338 can be modified significantly by such winds, and the corresponding modification in the
339 conductivity gradient can in turn modify the PRE vertical drift (Abdu et al., 2003; 2006;
340 Abdu and Brum 2009), a steeper gradient producing larger vertical drift.

341

342 The result in Fig.3 shows that the gravity wave induced polarization electric field wave
343 structures/oscillations occur nearly in a phase coherent way on the different days (for the
344 G1 group of days), which may point to some kind of interaction between the upward
345 propagating tides and gravity waves in their encounter probably at the base of the
346 thermosphere, or even higher up in the F region. As discussed by Fritts, et al. (2008) the
347 superposition of tidal and GW fields can produce regions in which eastward and
348 downward winds and electron density gradients become correlated and enhanced.
349 However, the nature of the interaction that can result in a coherent occurrence of the GW
350 oscillations, as observed in these results, is not clear at this time. Alternatively we can
351 imagine that interaction can occur through the well-known spatial resonance mechanism
352 (Klostermeyer, 1978; Huang and Kelley, 1996) by which a density or polarization electric
353 field perturbation can grow in amplitude when the phase speed of the gravity wave
354 becomes equal to the drift speed of the ionization. As discussed by Huang and Kelley
355 (1996) this mechanism can contribute to the growth of a seed perturbation that might
356 further lead to instability growth by the Rayleigh-Taylor mechanism under favorable
357 conditions of the post-sunset hours. The daytime increase of the wave amplitude in Fig.3
358 may as well be considered as an amplification of a precursor seed perturbation towards
359 sunset under the spatial resonance mechanism as discussed in the literature. The need to
360 invoke such a mechanism is two-fold: (a) as an additional factor to explain the wave
361 amplification towards sunset due to the fact that the field line integrated conductivity
362 ratio of Eq. 1 alone appears to be inadequate to explain the observed degree of
363 amplification in the polarization electric field during the same period; (b) The “phase
364 coherence” of the oscillations on the different days appears conceivable if the interacting
365 tidal mode wind field maintains the local time of its maximum nearly invariant on the
366 group of days that shows the coherence feature in the precursor wave structure. Even
367 though the spatial resonance condition should be similar on these different days the
368 precise nature of a tidal-gravity wave interaction in this case is unknown at this stage. It
369 appears relevant to point out in this context that Taori et al (2010) found in their case
370 study that wave amplification at tidal as well as gravity wave periods occurred between
371 86 km and 94 km (emission heights of OH and O2 lines, respectively) on two nights of
372 EPB occurrence as compared to EPB non occurrence nights. This may perhaps imply

373 some kind of connection between the tidal mode winds and the PRE, which is a key
374 factor (besides the gravity wave induced polarization electric field) in determining the
375 ESF instability growth.

376

377 The height variation in the amplitude of the polarization electric field wave structure (as
378 verified from the results at different plasma frequencies in Figs 1(a) and (c)) may be
379 explained on the basis of the possibility that the condition for spatial resonance can vary
380 with height depending upon the height variations in the plasma zonal speed and the GW
381 phase speed. We may note here that a relationship between the wave structure amplitude
382 (at the height of the 8MHz) and PRE vertical drift stands out clearly in the statistical
383 results of Fig.3 for the range of drift values varying from ~ 40 to 80 m/s (in their average
384 values) for the two groups considered. We have not verified here how well such a clear
385 relationship could be present if we consider days of smaller amplitudes for the PRE
386 vertical drift. It will be the focus of a follow up study. We may further point out here that
387 in investigations on the complementary contributions from the seed wave structure and
388 the PRE vertical drift for the ESF/bubble instability growth, we may expect to see
389 contrasting types of relationship between them on a case by case basis. For example, in a
390 case study of ESF instability growth under gravity wave seed perturbations and vertical
391 drifts, Abdu et al (2009a) found that for the PRE vertical drift peak values less than 30
392 m/s, the amplitude of the GW seed perturbation required for the instability growth was
393 larger (smaller) when the vertical drift was smaller (larger). Thus, further studies need to
394 be undertaken to establish the detailed nature of the connection between the precursor
395 wave structure (or the LSWS) and PRE vertical drift in the context of their competing
396 roles in the ESF development. It is to be emphasized here, on the basis of this study, that
397 an attempt to evaluate the role of a seed/precursor perturbation in ESF instability growth
398 should be based on the recognition that the role of the evening PRE vertical drift is a
399 complementary, and often dominating one, so that any study based only on one of these
400 precursor factors may lead to misleading results. We may make a comment here that the
401 wave structure phenomenon observed in this study over Brazilian equatorial region
402 should be observable with similar characteristics at other equatorial longitudes as well.

403

404 5- Conclusions

405

406 We have analyzed 1 to 2+ months of Digisonde data from three equatorial sites in Brazil
407 at a medium solar activity period epoch, seeking to understand better the nature of the
408 precursor wave structure (also known as LSWS) in the F layer heights that usually plays
409 important role, together with the PRE vertical drift, in the post sunset development of
410 spread F/bubble irregularities. The analysis is based on extracting the small amplitude
411 oscillations in the F layer heights at a number of plasma frequencies during the local time
412 period from midday to evening, that is, well before the sunset and the PRE development.
413 Very interesting results on the nature of the wave structure, its amplification towards
414 sunset and its relation with the PRE vertical drift were obtained, whose explanation is in
415 part tentative at present. The main conclusion of this study may be summarized as
416 follows: (1)- Gravity wave induced wave structures in polarization electric field in the
417 form of F layer height oscillations produced by the vertical or zonal perturbation winds is
418 a common feature in the equatorial region over Brazil during the period of the present
419 investigation; (2) The amplitudes of the wave structure, which we here call precursor
420 wave structure, also known in the literature as large scale wave structure (LSWS)
421 undergo systematic amplification during the afternoon till post sunset hours, leading to
422 spread F/plasma bubble irregularity development, on a statistical basis; the cases of non
423 occurrence of post sunset spread F are associated with lower amplitudes of the precursor
424 wave structure as also to lower values of the PRE vertical drift; (3) The sustenance of the
425 wave structure amplitude during the daytime is made possible by the significant value
426 (approaching unity) of the ratio of the field line integrated Pedersen conductivities of the
427 F region segment to the total field line including the E region segment, while the degree
428 of its amplification towards sunset appears to be partially dependent on the increase of
429 that ratio towards sunset; (4) There is a clear connection between the polarization electric
430 field wave structure amplitude and the PRE vertical drift velocity for average values of
431 the drift velocity in the range of 40 m/s to 80 m/s, larger wave structure amplitude
432 preceding larger vertical drift values (5) The wave structures having larger amplitudes
433 and larger degree of amplification towards sunset tend to occur nearly in-phase on the
434 different days considered; (6) As a tentative explanation, a significant part of the

435 amplitude growth towards sunset and the “phase coherence” of the wave structure on
436 different days are attributed to tidal– and gravity wave interaction involving possibly the
437 well known spatial resonance mechanism. Studies are underway for further elucidating
438 more detailed features of the precursor wave structure, including the nature of its
439 connection with the PRE vertical drift and the complementary roles they play in the post
440 sunset spread F/bubble development

441

442 Acknowledgements:

443 This work was supported by the Conselho Nacional de Desenvolvimento Científico e
444 Tecnológico (CNPq) through the process: CNPq no. 300883/2008–0. The data
445 analyzed in this paper was obtained from the Digisonde network operated by INPE.

446

447 References:

448 Abdu, M. A.; Brum, C.G.M.. Electrodynamics of the vertical coupling processes in the
449 atmosphere-ionosphere system of the low latitude region. *Earth, Planets and Space*, 61, p.
450 385-395, 2009.

451

452 Abdu, M. A., I. S. Batista, and J. A. Bittencourt (1981a), Some characteristics of spread F
453 at the magnetic equatorial station Fortaleza, *J. Geophys. Res.*, 86, 6836,
454 doi:10.1029/JA086iA08p06836.

455

456 Abdu, M. A., Bittencourt, J. A., Batista, I. S. (1981b) Magnetic declination control of the
457 equatorial F region dynamo field development and spread F, *J. Geophys. Res.*, 86, 11443-
458 11446.

459

460 Abdu, M. A., R. T. Medeiros, J. H. A. Sobral, and I. S. Batista (1983), Vertical ionization
461 drift velocities and range type spread F in the evening equatorial ionosphere, *J. Geophys.*
462 *Res.*, 88, 399–402.

463

464 Abdu, M. A., J. W. MacDougall, I. S. Batista, J. H. A. Sobral, and P. T. Jayachandran,
465 Equatorial evening prereversal electric field enhancement and sporadic E layer

466 disruption: A manifestation of E and F region coupling, *J. Geophys. Res.*, 108(A6),
467 1254, doi:10.1029/2002JA009285, 2003.

468

469 Abdu, M. A. P. P. Batista, I. S. Batista, C.G. M. Brum, A. Carrasco, B.W. Reinisch,,
470 Planetary wave oscillations in mesospheric winds, equatorial evening prereversal electric
471 field and spread F. *Geophys. Res. Letts.*, 33, L07107, doi:10.1029/2005GL024837, 2006
472

473 Abdu, M. A., Kherani, E. A., Batista, I. S., Batista, P. P., Paula, E. R. de Paula, Fritts, D.
474 Sobral, J.H.A., Gravity wave initiation of equatorial spread F/plasma bubble
475 irregularities based on observational data from the SpreadFEx campaign. *Annales*
476 *Geophysicae. Series A, Upper atmosphere and space sciences*, v. 27, p. 2607-2622,
477 2009a.

478

479 Abdu, M. A., I. S. Batista, B. W. Reinisch, J. R. de Souza, J. H. A. Sobral, T. R.
480 Pedersen, A. F. Medeiros, N. J. Schuch, E. R. de Paula, and K. M. Groves (2009b),
481 Conjugate Point Equatorial Experiment (COPEX) campaign in Brazil: Electrodynamics
482 highlights on spread F development conditions and day-to-day variability, *J. Geophys.*
483 *Res.*, 114, A04308, doi:10.1029/2008JA013749.

484

485 Abdu, M. A., E. A. Kherani, I. S. Batista, B. W. Reinisch, and J. H. A. Sobral (2013),
486 Equatorial spread F initiation and growth from satellite traces as revealed from conjugate
487 point observations in Brazil, *J. Geophys. Res. Space Physics*, 11, doi:10.1002/
488 2013JA019352.

489

490 Abdu, M. A., E. A. Kherani, I. S. Batista, B. W. Reinisch, and J. H. A. Sobral, (2014),
491 Equatorial spread F initiation and growth from satellite traces as revealed from conjugate
492 point observations in Brazil, *J. Geophys. Res. Space Physics*, 11 ,
493 doi:10.1002/2013JA019352.

494

495 Bailey, G. J., N. Balan, and Y. Z. Su (1997), The Sheffield University ionosphere-
496 plasmasphere model—A review, *J. Atmos. Terr. Phys.*, 59(13), 1541–1552.

497

498 Batista, I. S., M. A. Abdu, and J. A. Bittencourt (1986), Equatorial F region vertical
499 plasma drifts: Seasonal and longitudinal asymmetries in the American sector, *J. Geophys.*
500 *Res.*, 91, 12,055 – 12,064, doi:10.1029/JA091iA11p12055.

501

502 Bittencourt, J. A., Abdu, M. A. . Theoretical comparison between apparent and real
503 vertical ionization drift velocities in the equatorial F region, *J. Geophys. Res.*,86, 2451-
504 2455, 1981.

505

506 Carter, B. A., E. Yizengaw, J. M. Retterer, M. Francis, M. Terkildsen, R. Marshall, R.
507 Norman, and K. Zhang (2014), An analysis of the quiet time day-to-day variability in the
508 formation of postsunset equatorial plasma bubbles in the Southeast Asian region, *J.*
509 *Geophys. Res. Space Physics*, 119, 3206–3223, doi:10.1002/2013JA019570.

510

511 Eccles, J. V., A simple model of low-latitude electric fields, *J. Geophys.Res.*, 103,
512 26,699–26,708, 1998.

513

514 Farley, D. T., E. Bonelli, B. G. Fejer, and M. E. Larsen, The prereversal enhancement of
515 the zonal electric field in the equatorial ionosphere, *J. Geophys. Res.*, 91, 13,723-13,728,
516 1986.

517

518 Fejer, B. G., L. Scherliess, and E. R. de Paula (1999), Effects of the vertical plasma drift
519 velocity on the generation and evolution of equatorial spread F, *J. Geophys. Res.*, 104,
520 19,859–19,869.

521

522 Fritts, D. C., S. L. Vadas, D. M. Riggin, M. A. Abdu, I. S. Batista, H. Takahashi, A.
523 Medeiros, F. Kamalabadi, H.-L. Liu, B. G. Fejer, and M. J. Taylor, Gravity wave and
524 tidal influences on equatorial spread F based on observations during the Spread F
525 Experiment (SpreadFEx). *Ann. Geophys.*, 26, 3235–3252, 2008.

526

527 Heelis, R. A., P. C. Kendall, R. J. Moffet, D. W. Windle, and H. Rishbeth (1974),

528 Electrical coupling of the E- and F-regions and its effects on the F region drifts and
529 winds, *Planet. Space Sci.*, 22, 743–756, doi:10.1016/0032-0633(74)90144-5.
530

531 Heelis, R. A., G. Crowley, F. Rodrigues, A. Reynolds, R. Wilder, I. Azeem, and A.
532 Maute (2012), The role of zonal winds in the production of a pre-reversal enhancement in
533 the vertical ion drift in the low latitude ionosphere, *J. Geophys. Res.*, 117, A08308,
534 doi:10.1029/2012JA017547.
535

536 Huang, C. S. and Kelley, M. C., Nonlinear evolution of equatorial spread F 1. On the role
537 of plasma instabilities and spatial resonance associated with gravity wave seeding, *J.*
538 *Geophys. Res.*, 101, A1, 283-292, 1996.
539

540 Hysell, D. L., E. Kudeki, and J. L. Chau, (2005), Possible ionospheric preconditioning by
541 shear flow leading to equatorial spread F, *Annales Geophysicae*, 23, 2647-2655.
542

543 Kil, H., L. J. Paxton, and S.-J. Oh (2009), Global bubble distribution seen from OCSAT-
544 1 and its association with the evening prereversal enhancement, *J. Geophys. Res.*, 114,
545 A06307, doi:10.1029/2008JA013672.
546

547 Klostermeyer, J., Nonlinear investigation of the spatial resonance effect in the nighttime
548 equatorial F region, *J. Geophys. Res.*, 83, 3753, 1978.
549

550 Li, G., B. Ning, M. A. Abdu, W. Wan, and L. Hu (2012), Precursor signatures and
551 evolution of post-sunset equatorial spread-F observed over Sanya, *J. Geophys. Res.*, 117,
552 A08321, doi:10.1029/2012JA017820.
553

554 Lyon, A. J., N. J. Skinner, and R. W. Wright (1961), Equatorial spread F at Ibadan,
555 Nigeria, *J. Atmos. Terr. Phys.*, 21, 100, doi:10.1016/0021-9169(61)90104-0.
556

557 MacDougall, J., M. A. Abdu, I. Batista, R. Buriti, A. F. Medeiros, P. T. Jayachandran,
558 and G. Borba (2011), Spaced transmitter measurements of medium scale traveling

559 ionospheric disturbances near the equator, *Geophys. Res. Lett.*, 38, L16806, doi:10.1029/
560 2011GL048598.

561

562 McClure, J. P., S. Singh, D. K. Bambogye, F. S. Johnson, and H. Kil (1998), Occurrence
563 of equatorial F region irregularities: Evidence for tropospheric seeding, *J. Geophys. Res.*,
564 103, 29,119.

565 Patra, A. K., A. Taori, P. P. Chaitanya, and S. Sripathi (2013), Direct detection of
566 wavelike spatial structure at the bottom of the F region and its role on the formation of
567 equatorial plasma bubble, *J. Geophys. Res. Space Physics*, 118, 1196–1202,
568 doi:10.1002/jgra.50148.

569 Richmond, A. D., T.-W. Fang, and A. Maute (2015), Electrodynamics of the equatorial
570 evening ionosphere: 1. Importance of winds in different regions, *J. Geophys. Res. Space*
571 *Physics*, 120, doi:10.1002/2014JA020934.

572

573 Rishbeth, H. (1971), Polarization fields produced by winds in the equatorial F region,
574 *Planet. Space Sci.*, 19, 357 – 369, doi:10.1016/0032- 0633(71)90098-5.

575

576 Röttger, J. (1973), Wavelike structures of large scale equatorial spread F irregularities, *J.*
577 *Atmos. Terr. Phys.*, 35, 1195.

578

579 Sridharan, R., Bagiya, Mala S. , Sunda, S., Choudhary. R., Pant, T. K. , Jose, L., 2014.
580 First results on forecasting the spatial occurrence pattern of L-band scintillation and its
581 temporal evolution. *J. Atmos. Sol-Terr Phys.* 19, 53–62.

582

583 Taori, A., J. J. Makela, and M. Taylor (2010), Mesospheric wave signatures and
584 equatorial plasma bubbles: A case study, *J. Geophys. Res.*, 115, A06302,
585 doi:10.1029/2009JA015088.

586

587 Thampi, S. V., M. Yamamoto, R. T. Tsunoda, Y. Otsuka, T. Tsugawa, J. Uemoto, and M.
588 Ishii (2009), First observations of large-scale wave structure and equatorial spread F

589 using CERTO radio beacon on the C/NOFS satellite, *Geophys. Res. Letts.*, 36, L18111,
590 doi:10.1029/2009GL039887.

591

592 Tsunoda, R. T., and B. R. White (1981), On the generation and growth of equatorial
593 backscatter plumes: 1. Wave structure in the bottomside F layer, *J. Geophys. Res.*, 86,
594 3610.

595

596 Tsunoda, R. T. (2008), Satellite traces: An ionogram signature for large-scale wave
597 structure and a precursor for equatorial spread F, *Geophys. Res. Lett.*, 35, L20110,
598 doi:10.1029/2008GL035706.

599

600 Tsunoda, R. T. (2010), On equatorial spread F: Establishing a seeding hypothesis,
601 *J. Geophys. Res.*, 115, A12303, doi:10.1029/2010JA015564.

602

603 Tsunoda, R. T., M. Yamamoto, T. Tsugawa, T. L. Hoang, S. Tulasi Ram, S. V. Thampi,
604 H. D. Chau, and T. Nagatsuma (2011), On seeding, large scale wave structure, equatorial
605 spread F, and scintillations over Vietnam, *Geophys. Res. Lett.*, 38, L20102,
606 doi:10.1029/2011GL049173.

607

608 Tulasi Ram, S., M. Yamamoto, R. T. Tsunoda, S. V. Thampi, and S. Gurubaran (2012),
609 On the application of differential phase measurements to study the zonal large scale wave
610 structure (LSWS) in the ionospheric electron content, *Radio Sci.*, 47, RS2001,
611 doi:10.1029/2011RS004870.

612

613 Tulasi Ram, S., M. Yamamoto, R. T. Tsunoda, H. D. Chau, T. L. Hoang, B. Damtie, M.
614 Wassai, C. Y. Yatini, T. Manik, and T. Tsugawa (2014), Characteristics of large-scale
615 wave structure observed from African and Southeast Asian longitudinal sectors, *J.*
616 *Geophys. Res. Space Physics*, 119, 2288–2297, doi:10.1002/2013JA019712.

617

618

619 Figure Captions:

620

621 Fig. 1(a): Mass plots of the band-pass filtered the F layer true height (hF) oscillations
622 (DhF) at 5 MHz and 8 MHz plasma frequencies for October 2001 over Fortaleza (top and
623 middle panels). The gray segment of each DhF curve, starting on an average near 21:30
624 UT, represents range spread F (ESF) in progress. The cases of non occurrence of spread F
625 are highlighted by the continuation of color coded curves into the night. These days are
626 listed in top panel with the same color coding as that of the plotted curves. Bottom panel
627 shows the corresponding mass plot of the vertical drift, with the mean value shown as a
628 white curve.

629 Fig 1. (b): Plots of DhF and PRE vertical drift only for non spread F days.

630 Fig. 1 (c): Plots similar to Fig. 1 (a) but for the site Sao Luis. Please note that the results
631 for 03 October are shown in yellow curve (running on top) in the upper two panels and in
632 blue curve in the bottom panel.

633

634 Fig. 2(a): Band-pass filtered (with period band 0.5 – 1.5 hrs.) height oscillation at four
635 plasma frequencies, 5, 6, 7 and 8 MHz, plotted with each frequency cumulatively
636 displaced upward by 5 km with respect to the 5 MHz (green) curve.

637 Fig. 2(b): Dipole magnetic field lines in meridian plane and illustrative reflection heights
638 in the F region of the four plasma frequencies 5, 6, 7, and 8 MHz, as expected for the
639 case of a zonally propagating gravity wave whose wave front is aligned with the
640 magnetic north-south. The E layer is shown connected to the F region by field lines.

641 Fig. 2(c): An example illustrating the amplification of the oscillations from midday
642 towards post sunset hours, (indicated by the shaded area). In this example the
643 amplification appears to be larger at the lower frequency 5MHz (lower height) and
644 decreases as height increases.

645

646 Fig. 3: Band-pass filtered oscillations in F layer height at 8MHz over Cachimbo, from
647 midday to midnight, mass plotted for a group of days that shows near-coherence of the
648 oscillation phase on these days (upper panel), and those showing random phases (middle
649 panel). The grey segment of the individual curves represents spread F occurrence. The

650 bottom panel shows the F layer vertical drifts averaged for the two groups of days, the
651 red and blue curves corresponding to the first group and second group, respectively.

652

653 Fig. 4: The upper panel shows the field line integrated conductivity ratio, $\Sigma_F^P / (\Sigma_F^P + \Sigma_E^P)$,
654 plotted as a function the magnetic field line equatorial apex height versus local time. The
655 lower panel shows the monthly average values of the parameters $N_{e8\text{MHz}}$ (the electron
656 density at 8MHz plasma frequency, thick red line), the height of 8MHz plasma frequency
657 (blue curve), the NmE (thin red line) and the ratio $N_{e8\text{MHz}} / (N_{e8\text{MHz}} + \text{NmE})$ (bottom black
658 curve) for October 2001 over Fortaleza. Please note the upper and lower plots are aligned
659 in time, although the upper panel is in LT (45 °W) = UT- 3h

660

661

662

663

664

665

666

667

668

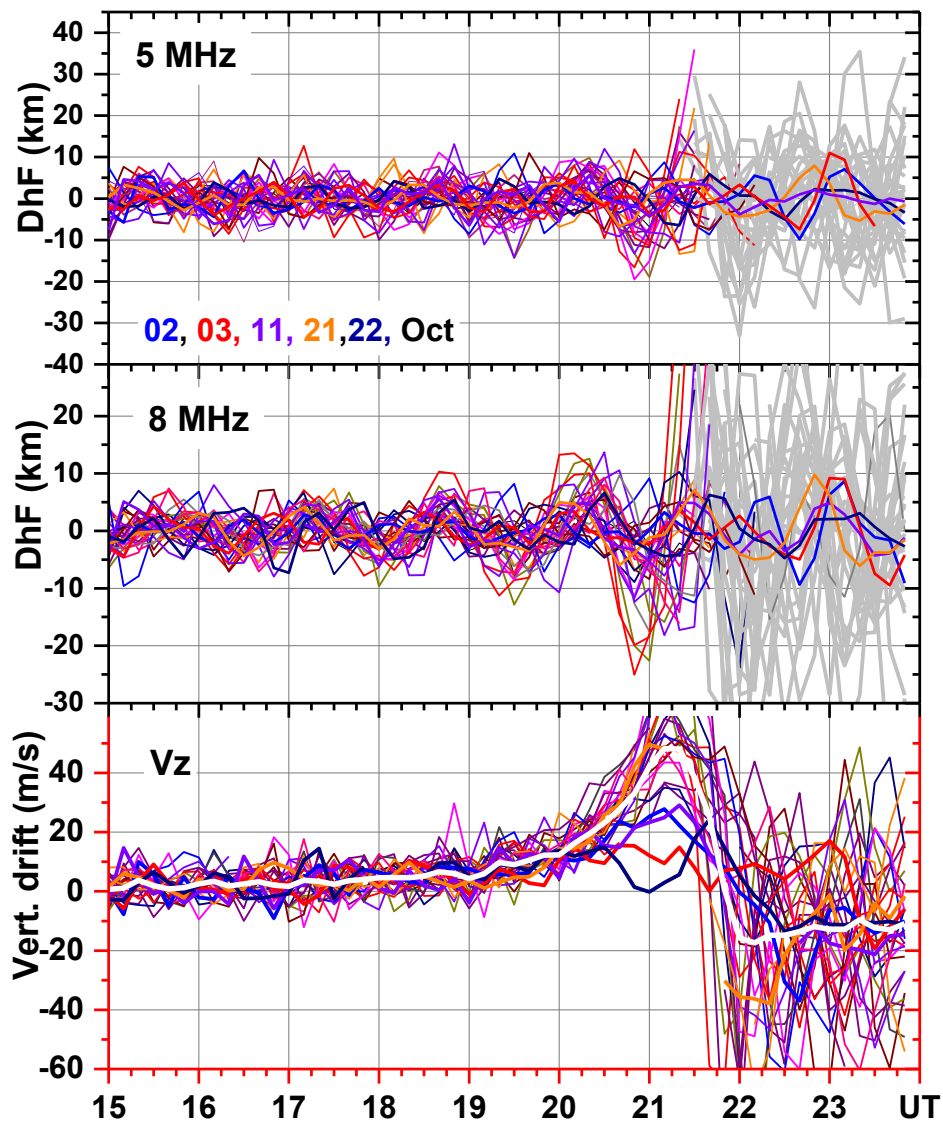
669

670

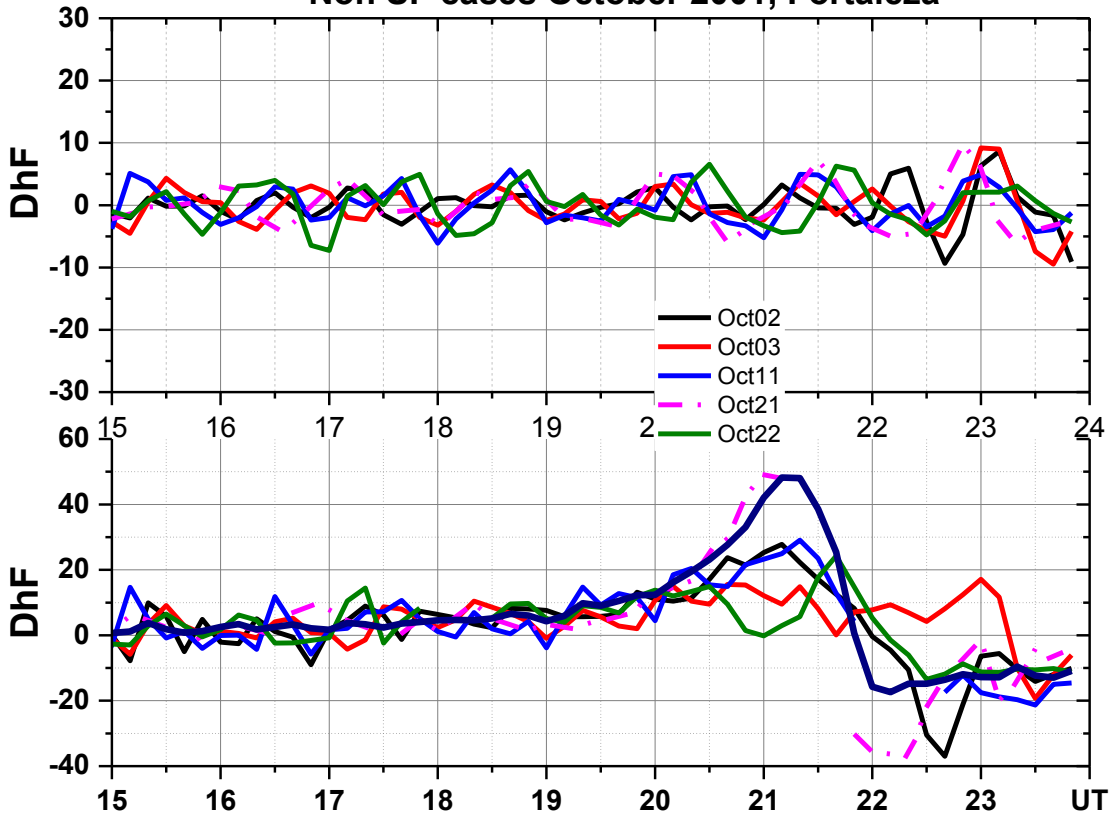
671

672

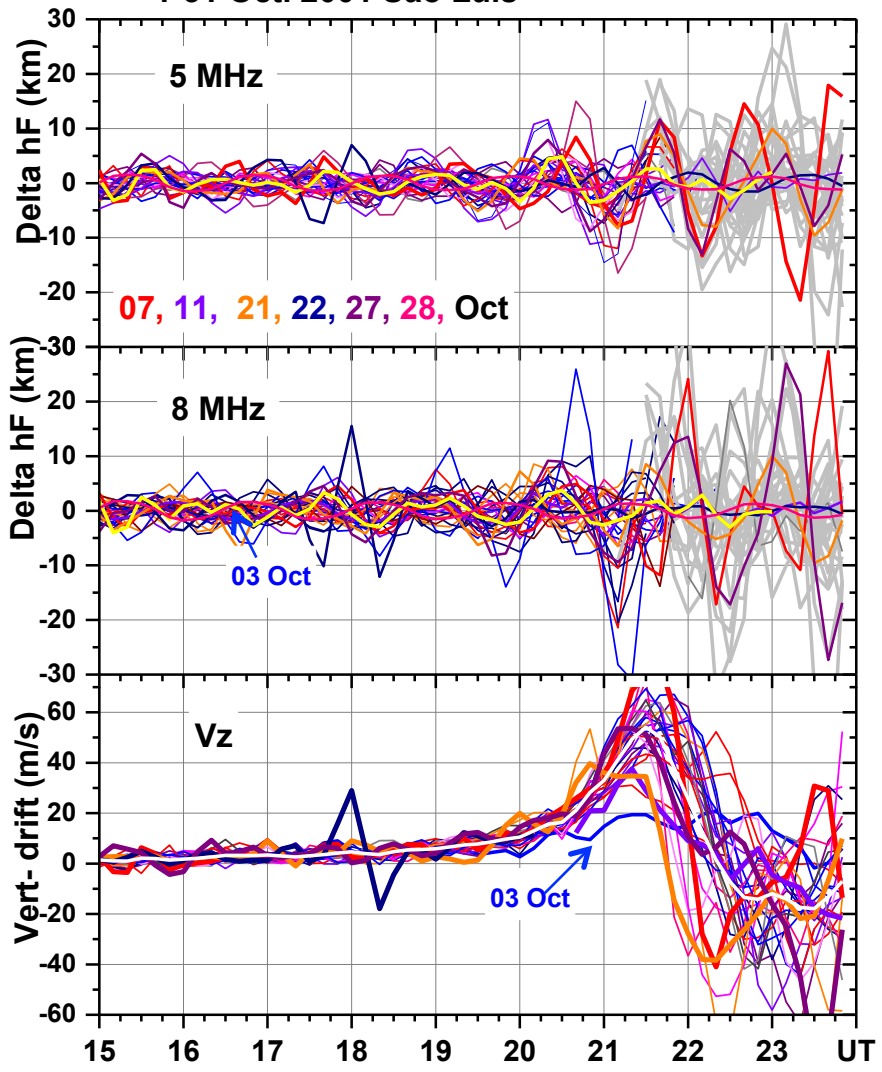
1-31 Oct 2001 Fortaleza

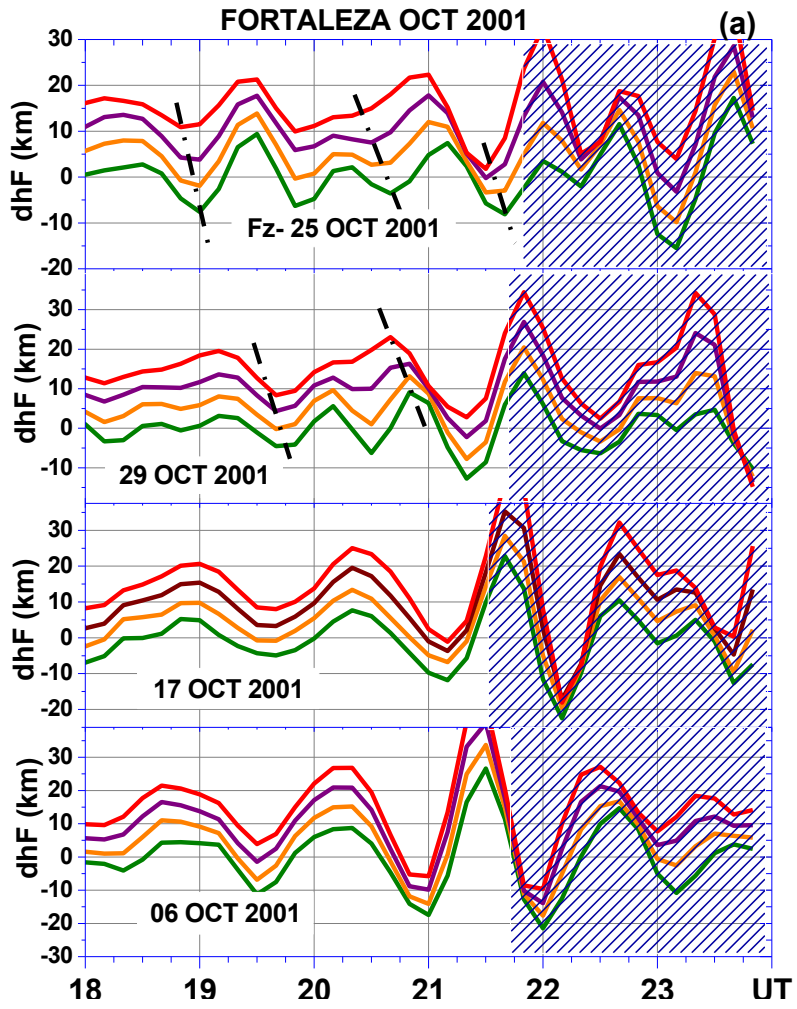


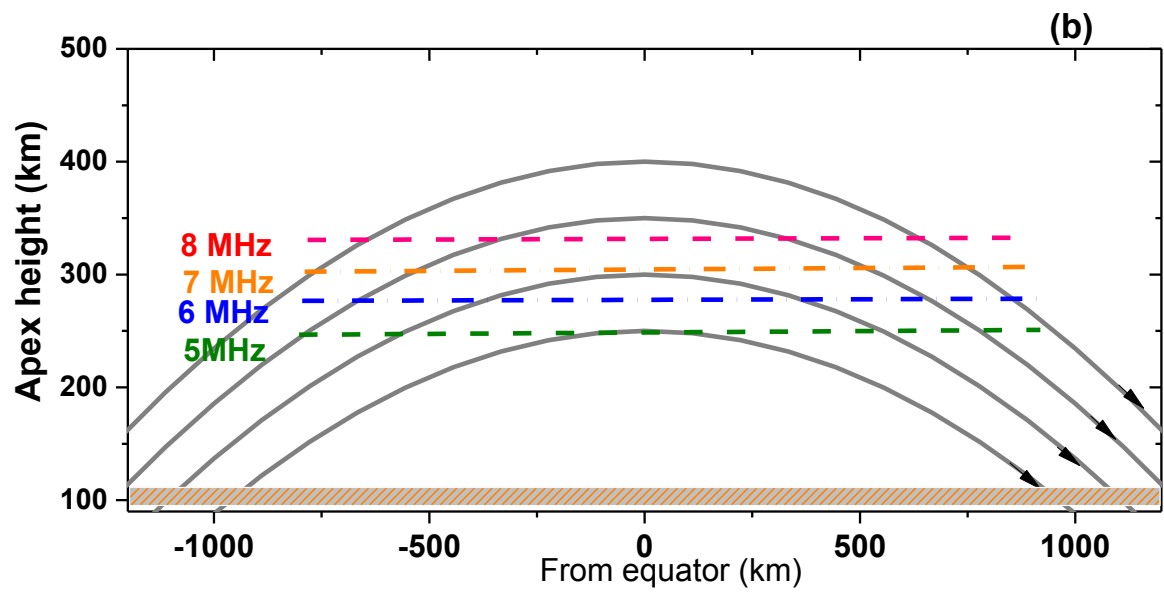
Non SF cases October 2001, Fortaleza

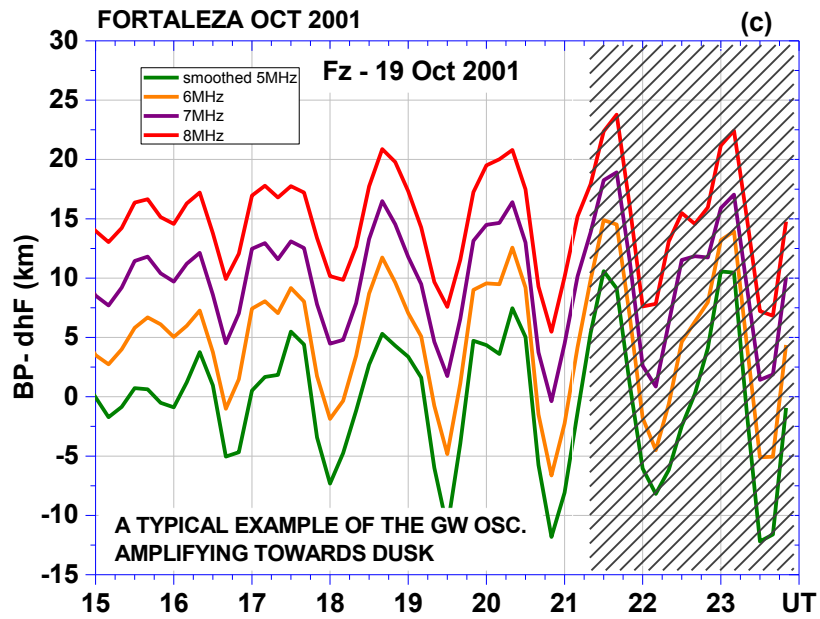


1-31 Oct. 2001 Sao Luis









Cachimbo, 1 Oct - 9 Dec 2002

